Room Temperature Exsolution of Cds Nanodots on A-site Deficient Cotton-Ball Like Titanate Perovskite Nanoparticles for H$_2$ Production Under Visible Light

Shreyasi Chattopadhyay, Aaron B Naden, William S. J. Skinner, Gwilherm Kerherve, David J Payne, and John T. S. Irvine*

Exsolution of nanoparticles followed by chemical treatment ("chemistry at a point") is a very exciting approach to the smart design of functional materials such as visible light active photocatalysts. Unfortunately, the usually utilized thermal reduction approach is not feasible for low melting point metals and compounds such as Cd and CdO. Here a hydrothermal approach to prepare exsolved CdS nanodots on cotton ball-like perovskite supports is described. The titanate-based photocatalyst is synthesized using a hydrothermal process followed by room-temperature sulfidation. The hydrothermal route directs A-site doping of Cd^{2+} via hydroxyl group incorporation in the titanate lattice. Formation of CdS via exsolution provides a high H$_2$ production mass activity of 3050 µmol g^{-1} h^{-1} under visible light with only 5 mol.% Cd doping of the titanate. Moreover, the strong CdS-support interaction offers good cycling stability under UV–vis and visible light irradiation. This is the first report describing the exsolution of CdS nanodots at room temperature and shows its advantages for photocatalytic activity.

1. Introduction

With increasing demand for decarbonization, renewable solar energy for the production of green H$_2$ fuel via photocatalytic water splitting continues to attract significant interest, providing a potential means for green energy storage.[1,2] Among various visible light-absorbing semiconductors, CdS with its band gap of ≈2.24 eV is a potential candidate for this purpose.[3,4] However, photo-corrosion is a serious drawback of CdS, therefore

S. Chattopadhyay, A. B Naden, J. T. S. Irvine
University of St Andrews
St Andrews, Fife KY16 9TS, UK
E-mail: jtsi@st-and.ac.uk
W. S. J. Skinner, G. Kerherve, D. J Payne
Department of Materials
Imperial College London
Exhibition Road, London SW7 2AZ, UK

several strategies are adopted to improve its stability.[5,6] Moreover, there are reports on loading noble metal co-catalysts like Pt or Au on CdS to achieve high-performance photocatalysts, at the expense of increased cost of the photocatalysts.[7,8] Here, we demonstrate a perovskite oxide system coupled with CdS to fabricate the desired photocatalyst for the promotion of the solar H$_2$ production rate by taking advantage of a synergistic effect of the components.[9–11] In this aspect, SrTiO$_3$ would be suitable as it allows modification of its physicochemical properties by tuning the stoichiometry through A or B site cation substitution.[9,12] Additionally, aliovalent La^{3+} doping results in A-site deficiency and hence lower the fermi level position, in turn increasing charge-carrier mobility and therefore influencing H$_2$ evolution activity.[13] Therefore, coupling these advantageous properties of (La$_x$Sr$_y$)TiO$_3$ with those of CdS, would provide a promising route to realizing an efficient catalytic system. However, the synthesis of Cd doped (La$_x$Sr$_y$)TiO$_3$ followed by exsolution of CdS is particularly challenging. Conventional high-temperature synthesis routes like the solid-state or pechini method are restricted by the low melting points of CdO and CdS. Because of this reason, a low-temperature sulfidation route is also necessary to exsolve out Cd^{2+} from the titanate lattice as CdS. To date, the concept of exsolution has largely been reported as thermal reduction leading to metal nanoparticles.[14] Such nanoparticles have undergone chemical reaction whilst remaining constrained at the surface in the phenomenon of "chemistry at a point" and this approach has been successfully applied to WS$_2$.[15,16] Therefore, this current work would provide a new direction of research.

Here, we have developed a novel low-temperature hydrothermal synthesis route to achieve Cd^{2+} doped La$_{0.4}$Sr$_{0.4}$TiO$_3$ followed by a room temperature sulfidation technique (Figure S2, Supporting Information) for in situ growth of CdS via exsolution. Furthermore, the visible light photoactivity of CdS exsolved photocatalysts was investigated and a superior mass activity for CdS content was observed.

Figure 1. Comparative a) XRD and b) FTIR analysis of 1) $La_{0.4}Sr_{0.4}Cd_{0.05}Ti_{0.95}O_{3-\delta}$, 2) $La_{0.4}Sr_{0.4}TiO_3$, and 3) $La_{0.4}Sr_{0.4}TiO_3$ (SS; c) TG analysis of $La_{0.4}Sr_{0.4}Cd_{0.05}Ti_{0.95}O_{3-\delta}$ in dry air. Inset of (a) shows change in cell parameter values.

2. Results and Discussion

$La_{0.4}Sr_{0.4}Cd_{0.05}Ti_{0.95}O_{3-\delta}$ was prepared hydrothermally at 190 °C followed by 400 °C treatment in the air for 2 h as described in the Figure S1, (Supporting Information). X-ray diffraction (XRD) (**Figure 1**a) of as-synthesized samples confirmed phase pure perovskite oxide with cubic (Pm-3m) crystal symmetry. A comparative study of XRD with $La_{0.4}Sr_{0.4}TiO_3$ fabricated by solid-state synthesis, $La_{0.4}Sr_{0.4}TiO_3$(SS), suggested cell expansion by showing increase in cell parameter value for hydrothermal (inset, Figure 1a) route in comparison to solid state method. It has been reported that such increment can be attained during hydrothermal reaction due to the incorporation of hydroxyl group in the lattice by replacing the oxygen vacancies.[17] Furthermore, broadening of diffraction peaks and shifting toward a higher 2θ value (inset, Figure 1a) on Cd^{2+} doping implies successful incorporation of Cd^{2+} in the framework with contraction of lattice parameter and cell volume. This is only possible when Cd^{2+} (0.95, 1.31 Å with coordination numbers VI and XII, respectively) with a lower ionic radius than Sr^{2+} (1.44 Å) and La^{3+} (1.36) occupies an A-site in the structure. Therefore, probably hydroxide group-assisted A-site doping of Cd^{2+} occurred.[18] No visible CdO-related peak was observed for $La_{0.4}Sr_{0.4}Cd_{0.05}Ti_{0.95}O_{3-\delta}$ further confirming the dissolution of Cd^+ in the lattice. Notably, the concentration of KOH solution was found to be crucial during synthesis to attain successful doping without any impurity. FTIR and TG analysis of the samples were further undertaken to ensure the fact of hydroxyl group incorporation. FTIR analysis (Figure 1b) showed presence of hydroxyl-related characteristics vibration bands at 3430 and 1646 cm^{-1} for $La_{0.4}Sr_{0.4}TiO_3$ and $La_{0.4}Sr_{0.4}Cd_{0.05}Ti_{0.95}O_{3-\delta}$, however, no such peaks were present for $La_{0.4}Sr_{0.4}Ti_{0.95}O_3$(SS).[19] The vibration peaks at 1370 cm^{-1} may arise from trace amounts of alcoholic -OH from ethylene glycol used during synthesis. The peaks in the range of 920–557 cm^{-1} are due to Ti-O vibrations.[20] As can be seen in Figure 1b, the peak at $\approx$810 cm^{-1} appears in the higher wavenumber region which may be due to the differences in crystallite size and the presence of -OH group. TG analysis (Figure 1c) also shows 1.96% weight loss in the temperature range 200–600 °C which corresponds to loss of $\approx$0.22 moles of [OH] from $La_{0.4}Sr_{0.4}Cd_{0.05}Ti_{0.95}O_{3-\delta}$. Therefore, these two results corroborated the XRD analysis suggesting incorporation of hydroxide group. Scanning electron microscopy (SEM)

of $La_{0.4}Sr_{0.4}Cd_{0.05}Ti_{0.95}O_{3-\delta}$ (**Figure 2**a,b) showed perovskite grains of $\approx$40–50 nm with unusual cotton ball-like morphologies. The magnified image in Figure 2b shows the presence of sheet-like structures aggregated to grow the hierarchical morphology. Scanning transmission electron microscopy (STEM) analysis (Figure 2c) further demonstrated the porous hierarchical structure of the perovskite grains. Figure 2d confirms the clear existence of nanosheets exposed on the surface of the cotton-ball-like nanoparticles. The atomic resolution image in Figure 2e shows the (pseudo)cubic arrangement of the metal ions where relatively larger bright spots and small lighter spots correspond to A and B site cations, respectively. Lattice fringes correspond to (110) plane with an interplanar spacing of $\approx$ 0.36 nm, higher than normal value can also be observed. Hence, we propose that during the hydrothermal synthesis, initially perovskite nanosheets are formed and those undergo self-aggregation to result in such a hierarchical structure, Figure 2f. EDX elemental mapping (Figure S3, Supporting Information) confirmed the homogenous distribution of the elements without any phase segregation and a composition corresponding to $La_{0.43}Sr_{0.49}Cd_{0.05}Ti_{0.95}O_x$ which is close to the expected composition. A small amount of potassium ($\approx$2 wt.%) was found as an impurity from the KOH used for synthesis. Since surface area is an important parameter to assess the photocatalytic activity of a photocatalyst, N_2 sorption analysis was performed to measure the specific surface area and porosity of $La_{0.4}Sr_{0.4}Cd_{0.05}Ti_{0.95}O_{3-\delta}$. A typical Type IV adsorption-desorption isotherm (Figure S4, Supporting Information) was obtained $La_{0.4}Sr_{0.4}Cd_{0.05}Ti_{0.95}O_{3-\delta}$ implying the presence of mesoporosity. The corresponding pore size distribution plot (inset, Figure S4, Supporting Information) was derived from the adsorption branch of the isotherm. BET surface area value of 54.55 m^2 g^{-1} and average pore diameter $\approx$10 nm with pore volume 0.28 cm^3 g^{-1} were calculated. Additionally, the presence of smaller pores of diameter $\approx$2 and 5 nm can also be seen in the pore size distribution plot.

Therefore, such a large surface area and porous structure would offer easy access to the active site for photocatalysis. To avoid any thermal treatment, a room-temperature sulfidation route was designed to exsolve CdS from the perovskite oxide framework (Figure S2, Supporting Information). A visible color change of $La_{0.4}Sr_{0.4}Cd_{0.05}Ti_{0.95}O_{3-\delta}$ from white to yellow powder (Figure S5, Supporting Information) suggested the

**ADVANCED
SCIENCE NEWS**

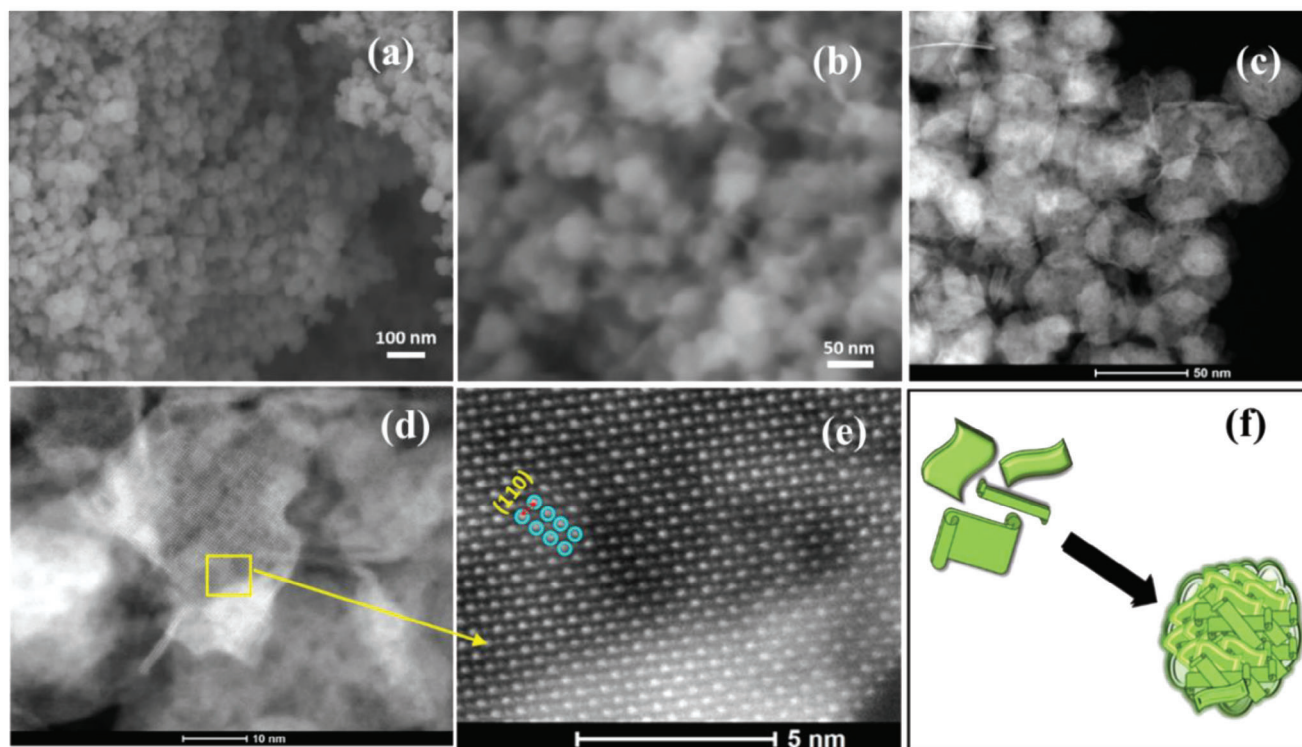www.advancedsciencenews.com

**ADVANCED
ENERGY
MATERIALS**

www.advenergymat.de

Figure 2. a,b) FESEM images of $La_{0.4}Sr_{0.4}Cd_{0.05}Ti_{0.95}O_{3-\delta}$ show the cotton-ball-like morphology. c,d) TEM analysis of $La_{0.4}Sr_{0.4}Cd_{0.05}Ti_{0.95}O_{3-\delta}$, e) HAADF image showing (110) atomic plane, f) schematic representation showing the probable route to hierarchical morphology.

formation of CdS on exsolution. It is noteworthy that diffusion of exsolving metal ions from deep inside the bulk to the surface is one of the crucial steps during exsolution.[21] This process requires a strong stimulus such as a concentration gradient or energy (i.e., temperature) to attain Gibb's free energy. In our case the affinity of Cd^{2+} for S^{2-} facilitated the diffusion of Cd^{2+} and simultaneously the unique nanoscale dimensions of the perovskite grains likely helped in lowering the free energy associated with such diffusion and exsolution. Moreover, the high porosity present on such hierarchical $La_{0.4}Sr_{0.4}Cd_{0.05}Ti_{0.95}O_{3-\delta}$ structures also played an important role in exsolution by providing escape sites. Therefore, we could achieve room tem-

perature exsolution of CdS on the surface. **Figure 3**a shows XRD pattern of the $La_{0.4}Sr_{0.4}Cd_{0.05}Ti_{0.95}O_{3-\delta}$ obtained after sulfidation. No CdS-related diffraction peaks were observed indicating small particle size of exsolved CdS. UV–Vis absorption spectroscopic technique was used to identify CdS exsolution. UV–Vis absorption spectrum of $La_{0.4}Sr_{0.4}Cd_{0.05}Ti_{0.95}O_{3-\delta}$ (Figure 3b) showed absorption only in UV range with an absorption maximum at ≈256 nm originating from the titanate component. Interestingly, there is a clear appearance of CdS absorbance band for $La_{0.4}Sr_{0.4}Cd_{0.05}Ti_{0.95}O_{3-\delta}$ with exsolved CdS. The corresponding spectrum showed a strong visible light absorption with a maximum of around 450 nm (Figure 3b) with
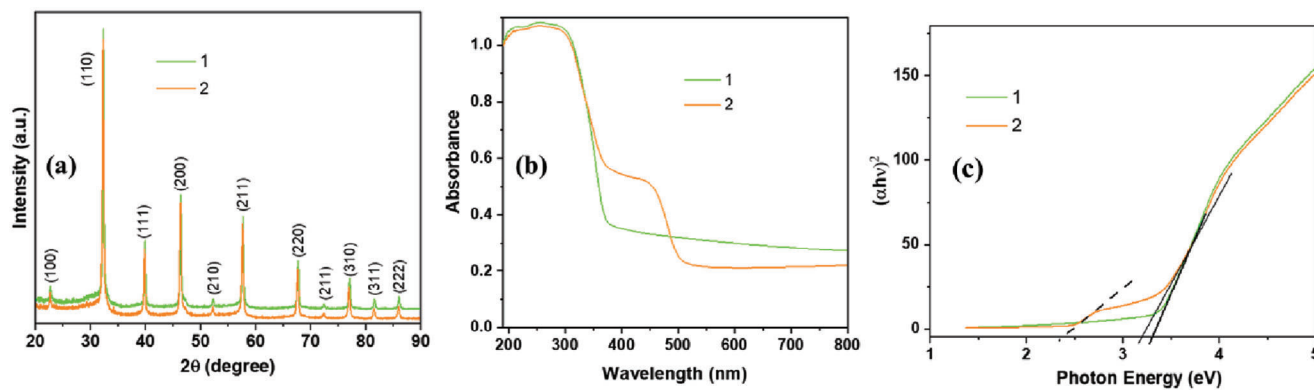

Figure 3. a) XRD patterns b) UV–Vis absorption spectra, and c) Tauc plot for band gap estimation of $La_{0.4}Sr_{0.4}Cd_{0.05}Ti_{0.95}O_{3-\delta}$ 1) before and 2) CdS exsolution.
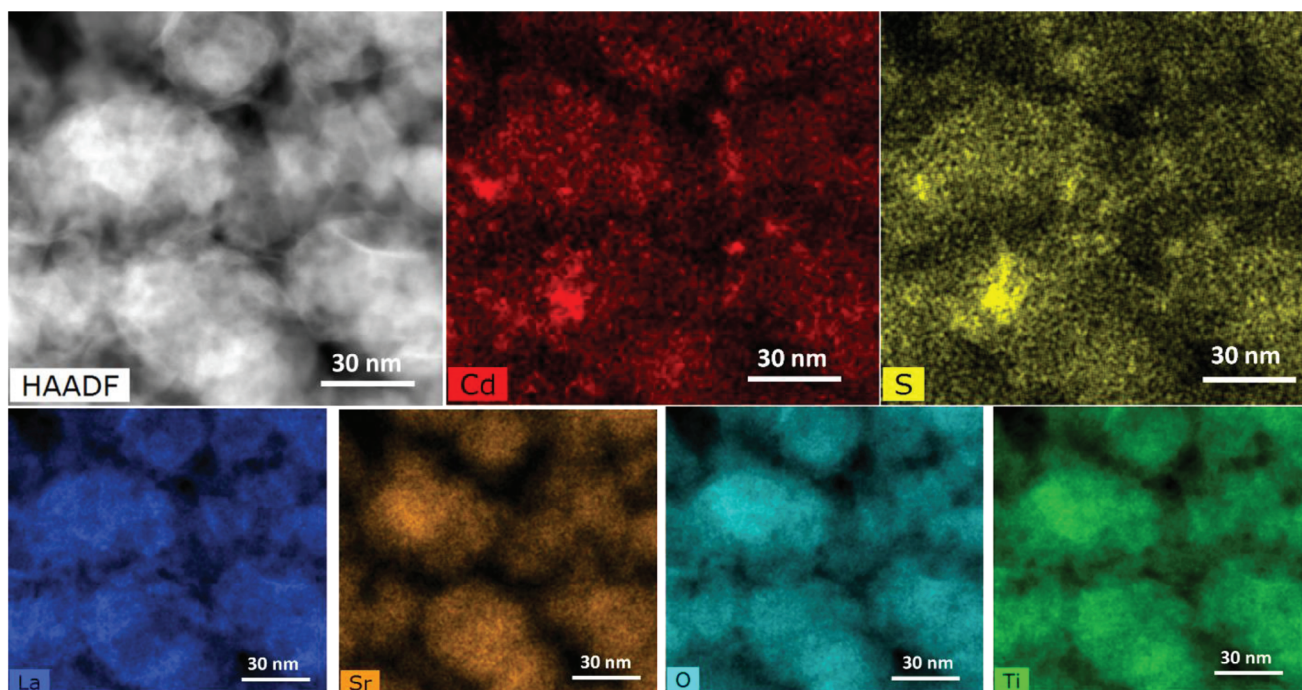
**ADVANCED
SCIENCE NEWS**

www.advancedsciencenews.com

**ADVANCED
ENERGY
MATERIALS**

www.advenergymat.de

Figure 4. TEM energy dispersive X-ray mapping of CdS exsoloved $La_{0.4}Sr_{0.4}Cd_{0.05}Ti_{0.95}O_{3-\delta}$ for distribution of La, Cd, S, Sr, O, Ti.

a red shifting of absorption band corresponding to the titanate component.

This result revealed the existence of CdS nanodots with a smaller band gap. Therefore, the color change of the powder from white to yellow along with the formation of CdS absorption in UV–vis absorption spectrum explicitly indicate the formation of CdS on exsolution.

Average particle size of exsolved CdS NPs was further calculated using Henglein's empirical formula (Equation. 1) and

$$2R_{(CdS)} = \frac{0.1}{(0.1338 - 0.0002345\lambda_a)} \tag{1}$$

found to be ≈3.5 nm. In the equation, R(CdS) and λa are the radii and absorption maxima of exsolved CdS nanodots. Band gap of $La_{0.4}Sr_{0.4}Cd_{0.05}Ti_{0.95}O_{3-\delta}$ before and after CdS exsolution was evaluated using the Tauc plot (Figure 3c) derived from by Kubelka-Munk transformation of UV–vis absorption spectra and extrapolating the linear part down to energy axis. The band gap values were found to be 3.31 and 3.19 eV for $La_{0.4}Sr_{0.4}Cd_{0.05}Ti_{0.95}O_{3-\delta}$ and $La_{0.4}Sr_{0.4}Cd_{0.05}Ti_{0.95}O_{3-\delta}$ with exsolved CdS, respectively. $La_{0.4}Sr_{0.4}Cd_{0.05}Ti_{0.95}O_{3-\delta}$ with exsolved CdS showed an additional E_g value at around 2.38 eV corresponding to the CdS nanodots. Therefore, exsolution of CdS led to the change in light absorption property of the material and was in good agreement with the color change observed after sulfidation. TEM analysis of CdS exsolved $La_{0.4}Sr_{0.4}Cd_{0.05}Ti_{0.95}O_{3-\delta}$ was performed to check the microstructure and element distribution after sulfidation reaction, **Figure 4**. Corresponding EDX elemental mapping showed a homogeneous distribution of all elements including cadmium and sulfur, coming from CdS. The quantification of the elements is summarized in Table S1, Supporting Infor-

mation. Under TEM it is very difficult to spot the nanodots as they are emerged on the thick perovskite oxide bulk surface. Moreover, the perovskite oxide nanoparticles are formed via accumulation of sheet-like structures which made it even more challenging to observe the CdS nanodot, and, for this reason, Cd and S dispersion in Figure 4 look agglomerated although in some parts small particles like dispersion can also be observed.

XPS measurements of the Sr 3d, Ti 2p, La 3d, Cd 3d, O 1s, and S 2p core levels were performed for $La_{0.4}Sr_{0.4}TiO_3$, $La_{0.4}Sr_{0.4}Cd_{0.05}Ti_{0.95}O_{3-\delta}$ and $La_{0.4}Sr_{0.4}Cd_{0.05}Ti_{0.95}O_{3-\delta}$ with exsolved CdS (**Figure 5**). The fitted core level spectra for each of these samples are provided in Figure S6, Supporting Information. The S 2p core level spectra were obtained by performing rapid measurements at various points across an area rather than at a single point, due to the observed decrease in sulfur intensity after prolonged exposure of the samples to the X-ray beam. The binding energies and relative atomic concentrations of the component elements and their respective chemical species are listed in Table 1. The plotted core level spectra were normalized to the area of the Sr $3d_{5/2}$ peak, owing to the fixed abundance of Sr and the consistent shape of the Sr 3d core level between the three samples, indicative of a constant chemical environment. The Sr 3d core levels (Figure 5a) of $La_{0.4}Sr_{0.4}TiO_3$, $La_{0.4}Sr_{0.4}Cd_{0.05}Ti_{0.95}O_{3-\delta}$, and $La_{0.4}Sr_{0.4}Cd_{0.05}Ti_{0.95}O_{3-\delta}$ with exsolved CdS were fitted with a single doublet, comprising the Sr $3d_{5/2}$ at a binding energy of ≈132.5 eV, separated from the higher binding energy Sr $3d_{3/2}$ component (Figure S6, Supporting Information) by a spin-orbit splitting of 1.75 eV. This doublet peak is attributed to lattice Sr^{2+} in all the samples.[22,23] A small difference of ±0.2 eV in the binding energy position of the Sr 3d doublet was observed between samples. This is within the expected error, and it is not considered to be indicative of any
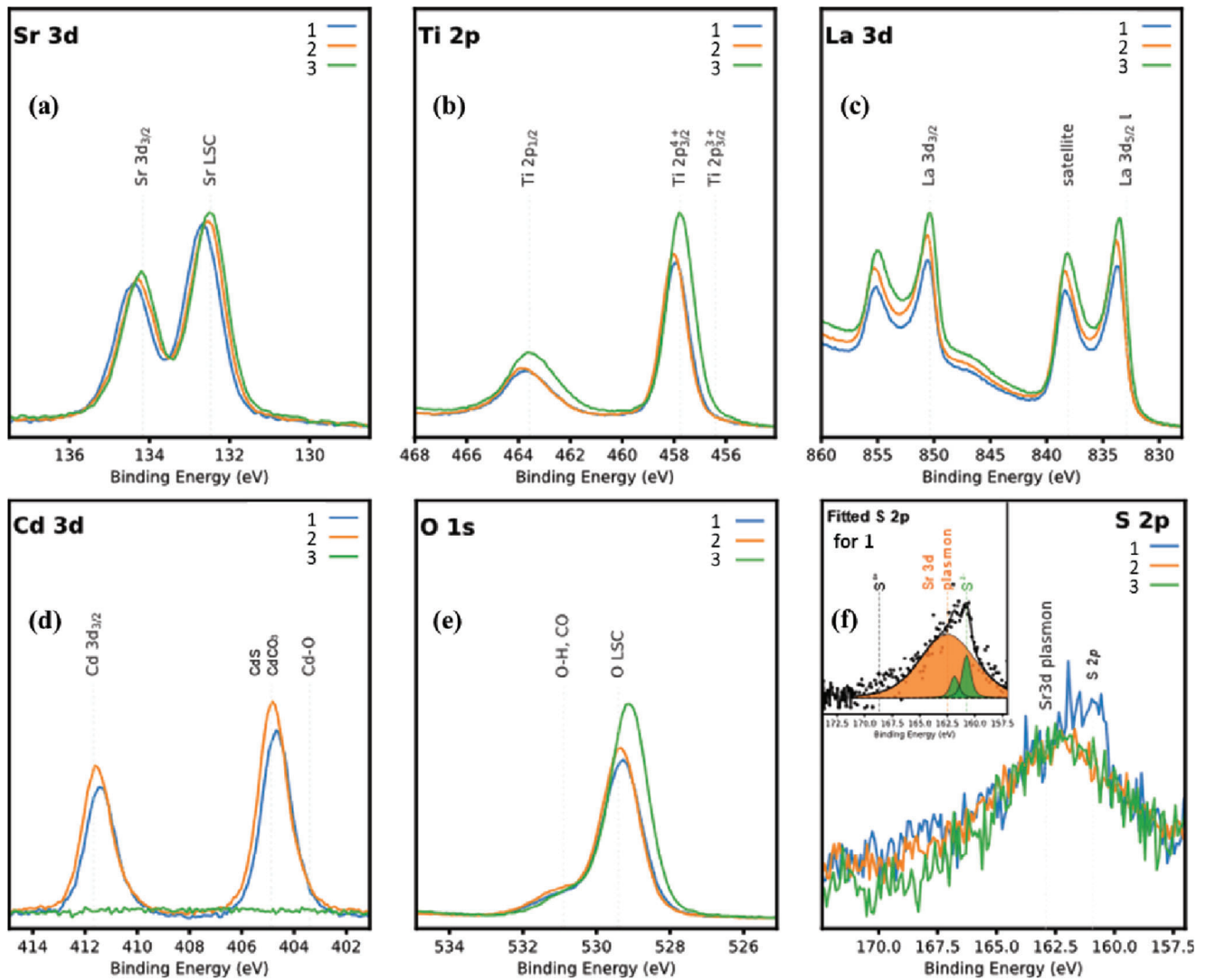
**ADVANCED
SCIENCE NEWS**

www.advancedsciencenews.com

**ADVANCED
ENERGY
MATERIALS**

www.advenergymat.de

Figure 5. XPS core level of the a) Sr 3d, b) Ti 2p, c) La 3d, d) Cd 3d, e) S 2p, f) O 1s for 1) CdS exsolved $La_{0.4}Sr_{0.4}Cd_{0.05}Ti_{0.95}O_{3-\delta}$ 2) $La_{0.4}Sr_{0.4}Cd_{0.05}Ti_{0.95}O_{3-\delta}$ and 3) $La_{0.4}Sr_{0.4}TiO_3$. The intensity of the spectra was normalized to the area of the Sr 3d5/2 peak.

Table 1. XPS binding energy values and atomic concentration of $La_{0.4}Sr_{0.4}TiO_3$, $La_{0.4}Sr_{0.4}Cd_{0.05}Ti_{0.95}O_{3-\delta}$, and CdS exsolved $La_{0.4}Sr_{0.4}Cd_{0.05}Ti_{0.95}O_{3-\delta}$.

	$La_{0.4}Sr_{0.4}TiO_3$		$La_{0.4}Sr_{0.4}Cd_{0.05}Ti_{0.95}O_{3-\delta}$		CdS exsolved $La_{0.4}Sr_{0.4}Cd_{0.05}Ti_{0.95}O_{3-\delta}$	
	BE [eV]	At. % Conc.	BE [eV]	At. % Conc.	BE [eV]	At. % Conc.
Sr $3d_{5/2}$ Sr-lat	132.5	8.4	132.6	9.8	132.7	10.9
Sr $3d_{5/2}$ Sr-surf	133.1	0.6	–	0.8	133.6	0.4
Ti $2p_{3/2}$ Ti^{3+}	456.2	2.32	456.2	2.0	456.4	2.1
Ti $2p_{3/2}$ Ti^{4+}	457.7	55.8	457.8	50.3	457.9	51.7
Cd $3d_{5/2}$ Cd-S, $CdCO_3$	–	–	404.7	2.2	404.7	2.1
Cd $3d_{5/2}$ Cd-O	–	–	403.6	0.2	403.8	0.2
La $3d_{5/2}$	833.6	32.8	–	34.7	833.8	32.3
S $2p_{3/2}$ S-Metal	–	–	–	–	160.6	0.3

chemical shift. Similar to previous work[23,24], a small amount of $SrCO_3$ was observed at a binding energy of 133.1 eV. The La 3d core level spectra (Figure 5c) of the three samples consist of a single doublet with well-separated spin-orbit components, which are split further by multiplet splitting.[25] The intensity ratio of the multiplet-split peaks of the La $3d_{5/2}$ component and 4.6 eV multiplet-splitting observed across all three samples are characteristic of La^{3+} in the form of La_2O_3.[22,23] Notably, the intensity of the La 3d core level peaks appears to consistently decrease between $La_{0.4}Sr_{0.4}TiO_3$, $La_{0.4}Sr_{0.4}Cd_{0.05}Ti_{0.95}O_{3-\delta}$, and $La_{0.4}Sr_{0.4}Cd_{0.05}Ti_{0.95}O_{3-\delta}$ with exsolved CdS, indicative of a decrease in the abundance of La relative to Sr at the surface between these samples.

The Ti $2p_{3/2}$ component of the Ti 2p core level (Figure 5b), separated from the Ti $2p_{1/2}$ component by a spin-orbit splitting of 5.7 eV, was fitted with two peaks at 457.8 and 456.3 ± 0.2 eV, corresponding to Ti^{4+} and Ti^{3+}, respectively (Figure S6, Supporting Information).[23] The calculated atomic percentage ratio of Ti^{3+}:Ti^{4+} remained consistent at $\approx$4: 96 at. %, between the three samples, indicative of a small amount of oxygen deficiency at the surface, with the reduction of Ti^{4+} to Ti^{3+} compensating the introduction of oxygen vacancies. The increase in intensity of the Ti 2p doublet of the undoped $La_{0.4}Sr_{0.4}TiO_3$ sample relative to the Cd-doped samples coincides with the substitution of Ti by Cd, resulting in a comparatively higher abundance of Ti. The Cd $3d_{5/2}$ component of the Cd 3d core level spectra (Figure 5d) of $La_{0.4}Sr_{0.4}Cd_{0.05}Ti_{0.95}O_{3-\delta}$ before and after CdS exsolution was fitted with two peaks at 404.7 and 403.7 eV (Figure S6, Supporting Information). The former is attributed to Cd^{2+} in CdS and $CdCO_3$, while the latter is attributed to Cd^{2+} in CdO. The intensity of the Cd 3d doublet appears to decrease between $La_{0.4}Sr_{0.4}Cd_{0.05}Ti_{0.95}O_{3-\delta}$ and $La_{0.4}Sr_{0.4}Cd_{0.05}Ti_{0.95}O_{3-\delta}$ with exsolved CdS, indicative of a decrease in the abundance of Cd relative to Sr at the surface between these samples. While the O 1s singlet (Figure 5e) demonstrates a similar decrease in intensity to Cd 3d, the intensity of the Ti 2p doublet remains constant between these two samples, suggesting that its relative abundance does not change. It is hypothesized that the slight reduction in peak intensity of the Cd 3d and O 1s signals between $La_{0.4}Sr_{0.4}Cd_{0.05}Ti_{0.95}O_{3-\delta}$ and $La_{0.4}Sr_{0.4}Cd_{0.05}Ti_{0.95}O_{3-\delta}$ with exsolved CdS, and corresponding decrease in abundance of Cd and O at the surface, is related to the presence of sulfur after CdS exsolution. Despite the S 2p core level being partially obscured by the overlapping Sr 3d plasmon (Figure 5f and Figure S5, Supporting Information), a contribution to the overall signal from S 2p is visible for $La_{0.4}Sr_{0.4}Cd_{0.05}Ti_{0.95}O_{3-\delta}$ with exsolved CdS and can be fitted with a single doublet peak, with the S $2p_{3/2}$ component (Figure 5f and Figure S5, Supporting Information) at 160.6 eV. This peak is attributed to the presence of S^{2-} in CdS based on previous XPS measurements, where the S $2p_{3/2}$ component of CdS was located at $\approx$161 eV.[24] Notably, no peak related to S^{6+} (168.7 eV) was observed, implying that the sample is free from any $CdSO_4$ impurities.[16,26] To correlate the S content obtained from EDS and XPS, we have calculated the S:Sr ratios from both XPS and TEM-EDS. The values were found to be S:Sr = 0.027 for XPS (Table 1) and S:Sr = 0.030 from EDS (Table S1, Supporting Information). It is noteworthy that, XPS is a surface technique and EDS is a bulk one. XPS results suggested that the surface of the perovskite became more Sr rich after exsolution. Therefore,

S:Sr ratios obtained from both analysis techniques are probably more reliable and are found to be same.

To verify the potential of $La_{0.4}Sr_{0.4}Cd_{0.05}Ti_{0.95}O_{3-\delta}$ with exsolved CdS towards H_2 evolution, $La_{0.4}Sr_{0.4}TiO_3$-CdS composite and bare CdS were synthesized as controls, and the corresponding XRD and UV–Vis absorption spectra are presented in Figure S7,S8, Supporting Information respectively. The photocatalytic activities of the catalysts were evaluated by monitoring the H_2 evolution under light irradiation of full range (λ > 300 nm) and visible light (λ > 400 nm) without any co-catalyst. It is noteworthy that suitable adsorption of sacrificial agent on the surface of photocatalyst is very crucial to control the H_2 evolution activity via removing photogenerated holes.

Therefore, we have chosen TEOA and N_2S/Na_2SO_3 pair to evaluate the H_2 production activity. Initial photocatalytic testing of all the catalysts was performed with 10% V TEOA solution (**Figure 6**). Under full range of light (λ > 300 nm), $La_{0.4}Sr_{0.4}Cd_{0.05}Ti_{0.95}O_{3-\delta}$ with exsolved CdS showed H_2 production rate 7 μmol g^{-1} h^{-1} which was almost 3 times higher than the rate of $La_{0.4}Sr_{0.4}TiO_3$ (Figure 6a). No significant difference was observed in photocatalytic activity for $La_{0.4}Sr_{0.4}Cd_{0.05}Ti_{0.95}O_{3-\delta}$ with exsolved CdS and $La_{0.4}Sr_{0.4}TiO_3$-CdS composite under UV–Visible light. However, an almost two times higher H_2 production rate was observed for CdS exsolved $La_{0.4}Sr_{0.4}Cd_{0.05}Ti_{0.95}O_{3-\delta}$ under visible light while comparing with $La_{0.4}Sr_{0.4}TiO_3$-CdS composite (Figure 6b). No H_2 was detected for $La_{0.4}Sr_{0.4}TiO_3$ under visible light (λ > 400 nm) using TEOA as sacrificial agent. The H_2 evolution activity of CdS exsolved $La_{0.4}Sr_{0.4}Cd_{0.05}Ti_{0.95}O_{3-\delta}$ was found to be lower than bare CdS (Figure 6) which might be due to the preferential strong attachment of TEOA on titanate perovskite surface rather than CdS[27] and could act as electron trapping sites. As a result, low H_2 production activity was observed. Whereas, for bare CdS, TEOA could get adsorbed on CdS surface but not that strongly to trap the electrons, hence, higher H_2 was obtained. Furthermore, it is reported that Na_2SO_3/Na_2S pair is an excellent sacrificial agent for CdS.28 It can effectively get adsorbed on CdS surface and the couple S^{2-} can successfully scavenge the photogenerated holes via oxidation where SO_3^{2-} restricts polysulfide formation, therefore, the photocatalytic H_2 evolution reaction can continue.[29] The H_2 production rate of CdS exsolved $La_{0.4}Sr_{0.4}Cd_{0.05}Ti_{0.95}O_{3-\delta}$ was found to be 189 and 118.34 μmol g^{-1} h^{-1} under full range (λ > 300 nm) and visible light (λ > 400 nm) when 0.1 м Na_2SO_3/Na2S was used as sacrificial agent. The control CdS sample showed an H_2 production rate of 338.314 and 127.12 μmol g^{-1} h^{-1} under full range and visible light. Interestingly, despite the very low CdS content in CdS exsolved $La_{0.4}Sr_{0.4}Cd_{0.05}Ti_{0.95}O_{3-\delta}$, the performance under visible light was comparable with bare CdS (Figure 6d). Further to check the cycling stability of the CdS exsolved $La_{0.4}Sr_{0.4}Cd_{0.05}Ti_{0.95}O_{3-\delta}$ photocatalyst, H_2 production was evaluated every 2 h (**Figure 7**a) without reintroducing the sacrificial agent. The stable performance of up to four cycles suggested good performance with cycling stability. It is noteworthy that in our $La_{0.4}Sr_{0.4}Cd_{0.05}Ti_{0.95}O_{3-\delta}$ photocatalyst, the amount of CdS content in 50 mg photocatalyst was 0.001934 g which was 4% with respect to bare CdS, and the CdS component was responsible for visible light absorption. Therefore, the mass activity of our CdS exsolved $La_{0.4}Sr_{0.4}Cd_{0.05}Ti_{0.95}O_{3-\delta}$ for the amount of CdS was calculated, and it reached 178.44 and
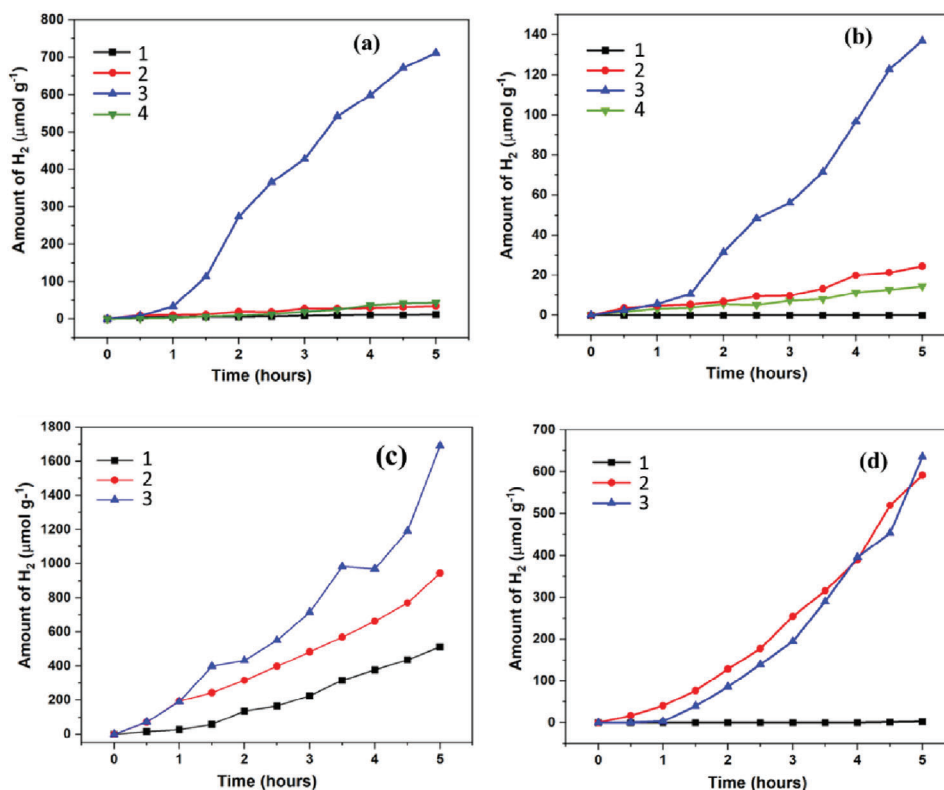
**ADVANCED
SCIENCE NEWS**

www.advancedsciencenews.com

**ADVANCED
ENERGY
MATERIALS**

www.advenergymat.de

Figure 6. Photocatalytic H_2 production rates using a,b) 10 v%TEOA and c,d) 0.1 M Na_2S/Na_2SO_3 as a sacrificial agent: under (a,c) Full range ($\lambda > 300$ nm) and (b,d) visible ($\lambda \geq 400$ nm) light (300 W Xe lamp). Plots (1), (2), (3) and (4) in Figure a,b represent $La_{0.4}Sr_{0.4}TiO_3$, CdS exsolved $La_{0.4}Sr_{0.4}Cd_{0.05}Ti_{0.95}O_{3-\delta}$, CdS and $La_{0.4}Sr_{0.4}Cd_{0.05}Ti_{0.95}O_{3-\delta}$-CdS composite, respectively. Plots (1), (2), and (3) in Figure c,d represents $La_{0.4}Sr_{0.4}TiO_3$, CdS exsolved $La_{0.4}Sr_{0.4}Cd_{0.05}Ti_{0.95}O_{3-\delta}$, and CdS, respectively All the experiments were done under vacuum with 50 mg photocatalyst and 100 ml water-sacrificial agent solution.

126.17 µmol g^{-1} h^{-1} under full range and visible light irradiation, respectively when 10% V TEOA was used as sacrificial agent (Figure S8, Supporting Information). These values were 1.2 and 4.5 times higher than bare CdS. Moreover, with 0.1 M Na_2S /Na_2SO_3 as a sacrificial agent, H_2 production rates of 4874 and 3058 µmol g^{-1} h^{-1} were obtained under full range and visible light, respectively, Figure 7b. Whereas, bare CdS exhibited 338.2 and 127.12 µmol g^{-1} h^{-1}, under full range and visible light, respectively. Therefore, almost 14 and 24 fold increases in mass activity for CdS amount were achieved. Furthermore, to prove the state of the art of this current work, the mass activity of CdS exsolved $La_{0.4}Sr_{0.4}Cd_{0.05}Ti_{0.95}O_{3-\delta}$ with reported values was also compared (Table S2, Supporting Information).[9,30–33] Furthermore, we have also compared our results with some previously reported Pt co-catalyst-loaded photocatalysts and summarized in Table S3, Supporting Information.[34–40] Such improvements in photocatalytic property revealed the influence of strong interaction between CdS nanodots and perovskite support which has been established by XPS. This intrinsic interaction retarded recombination rate by easy separation of electron and holes, and therefore facilitated successful utilization of photogenerated electrons. Moreover, the small particle size of perovskite NPs also helps in the fast separation of charge carriers and effective utilization of active sites. Hence, an improved photocatalytic H_2 production activity was achieved. To prove the stability of ex-

solved CdS on $La_{0.4}Sr_{0.4}Cd_{0.05}Ti_{0.95}O_{3-\delta}$, recovered photocatalysts were further characterized thoroughly after a water-splitting experiment under full range and visible light. UV–Vis (Figure S10, Supporting Information) showed no change in UV–Vis absorption edges after the photocatalysis reactions. TEM confirmed retention of microstructure and no elemental segregation or leaching was observed in corresponding EDX element mapping (Figure S11, Supporting Information), which proved the structural stability of CdS exsolved $La_{0.4}Sr_{0.4}Cd_{0.05}Ti_{0.95}O_{3-\delta}$. Moreover, the distribution of Cd and S over CdS nanodots of size $\approx$3-4 nm was also evaluated during line scanning (Figure S12, Supporting Information) under TEM. TEM elemental mapping (Figure S13, Supporting Information) of recovered samples after testing under visible light also confirmed the stability under such reaction conditions. It is noteworthy that, the EDS analysis presented in Figures S11,S13, (Supporting Information) show Cd: Sr ratios to be 0.110 and 0.10, respectively which is the same as the value obtained from Figure 4 before catalysis, Cd:Sr = 0.114. This justifies that there is almost no leaching of Cd in the solution. This result also supports the strong anchorage of CdS on perovskite support resulting from the exsolution that helps in protecting CdS, and therefore, suppresses photo-corrosion and leaching. Therefore, our approach not only offered enhanced photocatalytic activity but also assured photostability to our photocatalyst.
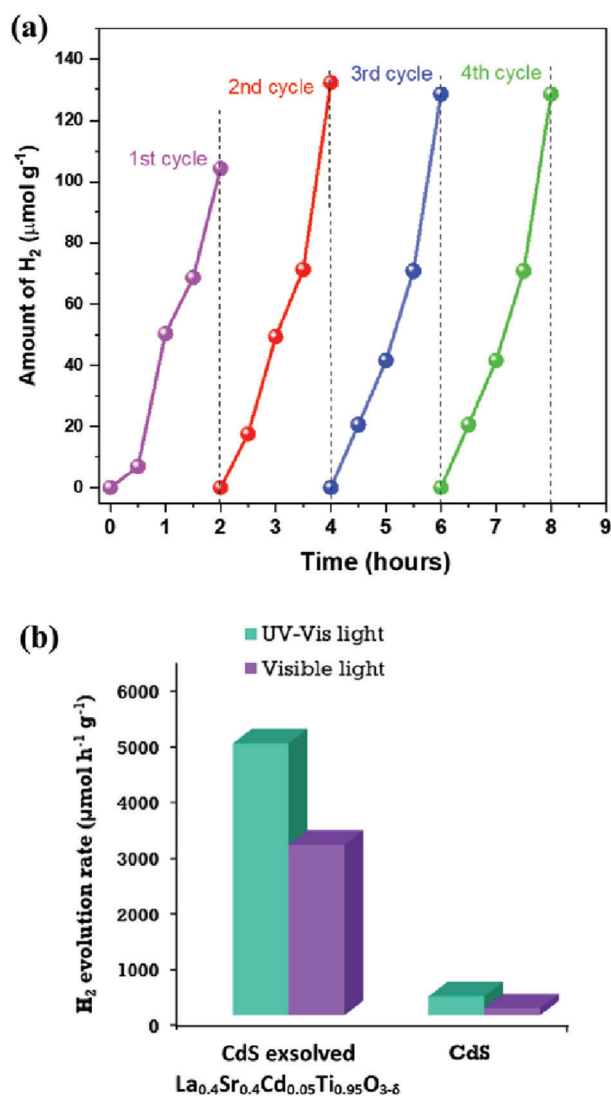
Figure 7. a) Cycling stability test under visible light ($\lambda \geq 400$ nm) and b) comparative mass activity for CdS content with 0.1 M Na2S /Na2SO3 sacrificial agent.

sented in this study can be applied for low-temperature exsolution of other catalytically active NPs and therefore demonstrates wide applicability.

Supporting Information

Supporting Information is available from the Wiley Online Library or from the author.

Conflict of Interest

The authors declare no conflict of interest.

Author Contributions

S.C. and J.T.S.I. conceived the concept and data analysis. S.C. designed the experiments, carried out sample preparation and photocatalytic water splitting study. A.B.N. collected TEM data and assisted in analysis. W.S.J.K., G.K., and D.J.P. performed XPS and analyzed the data. S.C. drafted the manuscript and all authors commented on it. J.T.S.I supervised the project.

Data Availability Statement

The research data underpinning this publication can be accessed at https://doi.org/10.17630/fb74f490-83ae-4c9d-b91e-8cc3f17b4fe1.[41]

3. Conclusion

We demonstrated a smart approach for room temperature exsolution of CdS nanodots on perovskite NPs. Hydrothermal synthesis route followed by low-temperature calcination yielded cotton ball-like perovskite NPs of size ≈40–50 nm with porosity that also created a high specific surface area. Such small particle size of perovskite with porous framework facilitated faster diffusion of Cd^{2+} ions and allowed to achieve room temperature sulfidation assisted CdS nanodot exsolution. Strong anchorage of CdS nanodots on perovskite support not only ensured photostability to CdS but also resulted in enhancement in photocatalytic H_2 production activity including under visible light which was confirmed by using different sacrificial agents. Therefore, this study has the potential for further development of the photocatalysts with improved activity. Moreover, the synthesis concept pre-

[1] V. H. Nguyen, H. H. Do, T. Van Nguyen, P. Singh, P. Raizada, A. Sharma, S. S. Sana, A. N. Grace, M. Shokouhimehr, S. H. Ahn, C. Xia, S. Y. Kim, Q. V. Le, *Sol. Energy* **2020**, *211*, 584.

[2] V. C. Nguyen, N. J. Ke, L. D. Nam, B.-S. Nguyen, Y. K. Xiao, Y. L. Lee, H. Teng, *J. Mater. Chem. A* **2019**, *7*, 8384.

[3] L. Cheng, Q. Xiang, Y. Liao, H. Zhang, *J. Energy Environ. Sci* **2018**, *11*, 1362.

[4] M. I. Ghouri, E. Ahmed, A. Ali, M. Ramzan, M. Irfan, *Mater. Sci. Semicond. Process.* **2021**, *122*, 105492.

[5] Y. Zhao, Y. Lu, L. Chen, X. Wei, J. Zhu, Y. Zheng, *ACS Appl. Mater. Interfaces* **2020**, *12*, 46073.

[6] M. Zhang, Y. Chen, J. N. Chang, C. Jiang, W. X. Ji, L. Y. Li, M. Lu, L. Z. Dong, S. L. Li, Y. P. Cai, Y. Q. Lan, *JACS Au* **2021**, *1*, 212.

[7] J. A. Nasir, Z. U. Rehman, S. N. A. Shah, A. Khan, I. S. Butler, C. R. A. Catlow, *J. Mater. Chem. A* **2020**, *8*, 20752.

[8] L. Ma, K. Chen, F. Nan, J. H. Wang, D.-J. Yang, L. Zhou, Q.-Q. Wang, *Adv. Funct. Mater.* **2016**, *26*, 6076.

[9] Y. Chang, K. Yu, C. Zhang, Z. Yang, Y. Feng, H. Hao, Y. Jiang, L. L. Lou, W. Zhou, S. Liu, *Appl. Catal. B Environ.* **2017**, *215*, 74.

[10] J. Xu, C. Sun, Z. Wang, Y. Hou, Z. Ding, S. Wang, *Chemistry* **2018**, *24*, 18512.

[11] H. Bian, D. Li, J. Yan, S. (Frank) Liu, *J. Energy Chem.* **2021**, *57*, 325.

[12] H. Irie, Y. Maruyama, K. Hashimoto, *J. Phys. Chem. C* **2007**, *111*, 1847.

[13] J. Hui, G. Zhang, C. Ni, J. T. S. Irvine, *Chem. Commun.* **2017**, *53*, 10038.

[14] D. Neagu, G. Tsekouras, D. N. Miller, H. Ménard, J. T. S. Irvine, *Nat. Chem.* **2013**, *5*, 916.

[15] D. Neagu, E. I. Papaioannou, W. K. W. Ramli, D. N. Miller, B. J. Murdoch, H. Ménard, A. Umar, A. J. Barlow, P. J. Cumpson, J. T. S. Irvine, I. S. Metcalfe, *Nat. Commun.* **2017**, *8*, 1855.

[16] Y.-F. Sun, Y. L. Yang, J. Chen, M. Li, Y.-Q. Zhang, J. H. Li, B. Hua, J.-L. Luo, *Chem. Commun* **2018**, *54*, 1505.

[17] J. G. Lee, A. B. Naden, C. D. Savaniu, P. A. Connor, J. L. Payne, J. M. Skelton, A. S. Gibbs, J. Hui, S. C. Parker, J. T. S. Irvine, *Adv. Energy Mater.* **2021**, *11*, 2101337.

[18] J. G. Lee, J.-H. Myung, A. B. Naden, O. S. Jeon, Y. G. Shul, J. T. S. Irvine, *Adv. Energy Mater.* **2020**, *10*, 1903693.

[19] Y. Ma, Z. Wu, H. Wang, G. Wang, Y. Zhang, P. Hu, Y. Li, D. Gao, H. Pu, B. Wang, X. Qi, *CrystEngComm* **2019**, *21*, 3982.

[20] A. M. Youssef, H. K. Farag, A. El-Kheshen, F. F. Hammad, *Silicon* **2018**, *10*, 1225.

[21] O. Kwon, S. Joo, S. Choi, S. Sengodan, G. Kim, *J. Phys. Energy*, *2*, 032001.

[22] M. I. Sosulnikov, Y. A. Teterin, *J. Electron Spectros. Relat. Phenomena* **1992**, *59*, 111.

[23] D. Neagu, T. S. Oh, D. N. Miller, H. Ménard, S. M. Bukhari, S. R. Gamble, R. J. Gorte, J. M. Vohs, J. T. S. Irvine, *Nat. Commun.*, *6*, 8120.

[24] X. R. Yu, F. Liu, Z. Y. Wang, Y. Chen, *J. Electron Spectros. Relat. Phenomena* **1990**, *50*, 159.

[25] M. F. Sunding, K. Hadidi, S. Diplas, O. M. Løvvik, T. E. Norby, A. E. Gunnæs, *J. Electron Spectros. Relat. Phenomena* **2011**, *184*, 399.

[26] Y. Hou, Y. Zhu, Y. Xu, X. Wang, *Appl. Catal. B Environ.* **2014**, *156–157*, 122.

[27] H. Nagakawa, M. Nagata, *ACS Omega* **2021**, *6*, 4395.

[28] Y. J. Yuan, D. Chen, Z. T. Yu, Z. G. Zou, *J. Mater. Chem. A* **2018**, *6*, 11606.

[29] M. Wang, S. Shen, L. Li, Z. Tang, J. Yang, *J. Mater. Sci.* **2017**, *52*, 5155.

[30] T. Feng, H. Li, R. Gao, G. Su, W. Wang, B. Dong, L. Cao, *ChemSusChem* **2022**, *15*, 202200288.

[31] S. R. Kadam, S. W. Gosavi, B. B. Kale, N. Suzuki, C. Terashima, A. Fujishima, *Sci. Rep.* *9*, 12036.

[32] B. Qiu, Q. Zhu, M. Du, L. Fan, M. Xing, J. Zhang, *Angew. Chemie – Int. Ed.* **2017**, *56*, 2684.

[33] G. Li, T. Xu, R. He, C. Li, J. Bai, *Appl. Surf. Sci.* **2019**, *495*, 143642.

[34] M. Khan, S. Woo, O. Yang, *Int. J. Hydrogen Energy* **2008**, *33*, 5345.

[35] T. Sreethawong, S. Laehsalee, S. Chavadej, *Catal. Commun.* **2009**, *10*, 538.

[36] H. Park, W. Choi, M. R. Hoffmann, *J. Mater. Chem.* **2008**, *18*, 2379.

[37] N. P. Tangale, P. S. Niphadkar, V. Samuel, S. S. Deshpande, P. N. Joshi, S. V. Awate, *Mater. Lett.* **2016**, *171*, 50.

[38] T. Puangpetch, T. Sreethawong, S. Yoshikawa, S. Chavadej, *J. Mol. Catal. A Chem.* **2009**, *312*, 97.

[39] Y.-Y. Tai, J. C. S. Wu, W. Y. Yu, M. M. Krzmanc, E. Kotomin, *Appl. Catal. B Environ.* **2022**, *324*, 122183.

[40] S. C. Erwin, L. Zu, M. I. Haftel, A. L. Efros, T. Kennedy, J. N. Doping, *Nat. Mater.* **2009**, *8*, 76.

[41] S. Chattopadhyay, A. B. Naden, W. S. J. Skinner, G. Kerherve, D. J. Payne, J. T. S. Irvine, Room temperature exsolution of CdS nanodots on A-site deficient cotton-ball like titanate perovskite nanoparticles for H_2 production under visible light. Dataset. University of St Andrews Research Portal, **2023**, https://doi.org/10.17630/fb74f490-83ae-4c9d-b91e-8cc3f17b4fe1.